Eur. Phys. J. C (2026) 86:96
https://doi.org/10.1140/epjc/s10052-026-15315-w

THE EUROPEAN PHYSICAL JOURNAL C

Regular Article - Theoretical Physics

A new Rényi holographic dark energy model and its cosmological implications

Zeinab Tamri[1,a], **Ali Aghamohammadi**[1,b], **Tayeb Golanbari**[2,c], **Abdolhosein Khodam-Mohammadi**[3,d]

[1] Department of Physics, Sa.C., Islamic Azad university, Sanandaj, Iran
[2] Department of Physics, University of Kurdistan, P.O. Box 66177-15175 Sanandaj, Kurdistan, Iran
[3] Department of Physics, Bu-Ali Sina University, P.O. Box 65178 Hamedan, Iran

Received: 29 November 2025 / Accepted: 10 January 2026

Abstract We develop a generalized holographic dark energy model based on the Rényi entropy, which introduces a logarithmic deformation of the Bekenstein–Hawking entropy and is characterized by a non-extensivity parameter α. By adopting the future event horizon as the infrared cutoff, we formulate the New Rényi Holographic Dark Energy (NRHDE) scenario and derive a modified holographic energy density that reduces smoothly to the standard HDE limit for $\alpha \to 0$. Starting from the Rényi entropy formalism, we obtain a closed and self-consistent set of evolution equations for the dark energy density parameter Ω_d, the equation-of-state parameter w_d, and the deceleration parameter q. We perform a detailed numerical investigation of the background dynamics over a physically reasonable range of the holographic parameter c and the Rényi deformation parameter α, and show that the NRHDE model predicts a late-time phantom regime over an extended region of the (c, α) parameter space, with a smooth approach toward the cosmological-constant boundary $w_d = -1$ as either parameter increases. We further provide a global characterization of the parameter space by means of two-dimensional maps of the present-day equation-of-state parameter and the transition redshift, which clarify the joint impact of (c, α) on the late-time cosmological evolution. Finally, a qualitative comparison between the NRHDE background predictions and observational Hubble data from cosmic chronometers is presented as a consistency check of the model at the background level. The NRHDE framework therefore constitutes a minimal and thermodynamically motivated extension of holographic dark energy, offering a flexible platform for future quantitative tests with late-time expansion data.

1 Introduction

Observations from Type Ia supernovae (SNe Ia) [1,2], the cosmic microwave background (CMB) anisotropies measured by *Planck* [3,4], and baryon acoustic oscillations (BAO) [5] have firmly established that the Universe is presently undergoing a phase of accelerated expansion. This behaviour is conventionally attributed to a dominant component with negative pressure, referred to as dark energy (DE). Despite extensive efforts over the past two decades, the physical origin of DE remains unknown, motivating a wide variety of theoretical proposals [3,6,7] as well as continued exploration of alternative cosmological frameworks. Among these, the holographic dark energy (HDE) scenario has received considerable attention [8–13].

The HDE framework is rooted in the holographic principle, which arises from black hole thermodynamics and connects entropy bounds to spacetime dynamics [10,11,14–16]. In this construction, the dark energy density is determined by the reduced Planck mass and an infrared (IR) cutoff length scale [8,9,17]. Different choices of this cutoff, such as the Hubble horizon, the particle horizon, the future event horizon, or the Granda–Oliveros cutoff, lead to distinct realizations of HDE models [8,9,17–21]. In this work we adopt the future event horizon as the IR cutoff, a choice widely investigated in the literature and known to naturally generate late-time cosmic acceleration [8,22–25]. This choice is particularly relevant in the presence of Rényi-type entropy corrections, since the additional positive contribution proportional to L^2 in the NRHDE energy density enhances the future-

[a] e-mail: zeinabta4@gmail.com
[b] e-mail: ali.aghamohamadi@iau.ac.ir (corresponding author)
[c] e-mail: t.golanbari@uok.ac.ir
[d] e-mail: khodam@basu.ac.ir

Published online: 31 January 2026

horizon-driven acceleration mechanism [26–29]. Based on this idea, HDE has been formulated and tested against various cosmological data [6,22,30–32].

The Hubble horizon is a dynamic scale that is related to the expansion rate of the universe and leads to an incorrect equation of state. Therefore, the future event horizon, which is complementary to the particle horizon, has been proposed as the foundation for holographic dark energy models, so clarified in the recent analysis of Manoharan [33], the infrared cutoff should be regarded as part of the model definition rather than as an *a priori* imposition of cosmic acceleration. Once the cutoff is specified, the cosmological dynamics follow self-consistently from the Friedmann equations, and the horizon evolution can be expressed locally as $\dot{r}_h = Hr_h - 1$, avoiding any explicit dependence on future boundary conditions.

Because gravity is intrinsically long-ranged and the microscopic structure of spacetime remains unknown, several generalized entropy formalisms have been proposed to describe gravitational and cosmological systems [23,24,34,35]. In addition to the standard Bekenstein–Hawking entropy, notable extensions include the Tsallis [36–38], Rényi [26,39,40], Barrow [27], Sharma–Mittal [41], and Kaniadakis [28,42,43] entropies. These non-extensive generalizations introduce characteristic deformations in the entropy–area relation, which in turn modify the associated holographic energy densities and can lead to non-trivial departures from the standard late-time expansion history.

Cosmographic reconstructions indicate that the impact of non-extensive entropy corrections is typically small at low redshift but becomes more pronounced toward intermediate and high redshifts, at least at the background level.

Recent studies have further shown that updated BAO and $H(z)$ data, including DESI results, can be used to probe mildly non-extensive holographic scenarios quantitatively [45–47]. While Tsallis holographic dark energy (THDE) has been extensively explored in this context [25,48–51], Rényi-based holographic constructions remain comparatively less studied, especially when the future event horizon is adopted as the infrared cutoff.

This work complements previous thermodynamic constructions (e.g., [29,52]) by adopting the future event horizon in the standard HDE framework. Motivated by this gap, we formulate and investigate a new Rényi-entropy-based holographic dark energy model, referred to as the New Rényi Holographic Dark Energy (NRHDE) scenario. The central novelty of the model is that the logarithmic deformation induced by Rényi entropy modifies the standard HDE density through a single non-extensivity parameter α, while preserving a smooth reduction to conventional HDE in the limit $\alpha \to 0$.

Starting from the Rényi entropy formalism, we derive a closed and self-consistent set of background evolution equations for the density parameter Ω_d, the equation-of-state parameter w_d, and the deceleration parameter q. We then perform a detailed numerical analysis over physically reasonable ranges of the holographic parameter c and the Rényi deformation parameter α. The model naturally predicts a late-time phantom regime over an extended region of the (c, α) parameter space, with a smooth approach toward the cosmological constant boundary $w_d = -1$ as either parameter increases. Although α is expected to be extremely small in fundamental units, in the normalized variables adopted here ($H_0 = 1, M_p = 1$) it can effectively be of order unity, rendering the NRHDE framework phenomenologically accessible at the background level.

The remainder of this paper is organized as follows. Section 2 presents the formulation of the NRHDE model and the derivation of the corresponding evolution equations. In Sect. 3 we analyze the cosmological dynamics and illustrate how (α, c) control the behaviour of Ω_d, w_d, and q. Our conclusions and future perspectives are summarized in Sect. 4. For completeness, the observational Hubble data used for the qualitative comparison are listed in Appendix A.

2 New Rényi holographic dark energy

The New Rényi Holographic Dark Energy (NRHDE) model provides an extended formulation of the conventional holographic dark energy (HDE) scenario through the incorporation of Rényi entropy into the holographic principle [26,53]. In the standard case, the Bekenstein-Hawking entropy establishes a linear relation between entropy and the horizon area. In contrast, Rényi entropy introduces a logarithmic correction governed by the non-extensivity parameter α, thereby modifying the entropy-area relation in a nontrivial manner. This leads to a generalized, entropy-motivated expression for the dark energy density that accounts for possible non-extensive and quantum-gravitational effects on cosmological scales. Importantly, the NRHDE model is continuously connected to the standard HDE in the limit $\alpha \to 0$.

Rényi entropy is defined as

$$S_R = \frac{1}{\alpha} \ln(1 + \alpha S_{BH}) , \tag{1}$$

where $S_{BH} = A/(4G)$ is the Bekenstein-Hawking entropy associated with a horizon of area $A = 4\pi L^2$, and L is the infrared (IR) cutoff, taken here to be the future event horizon. Expanding this expression for small αS_{BH} explicitly shows that Rényi entropy introduces systematic higher-order corrections beyond the standard entropy [25,26,51]. Applying the holographic relation between entropy and energy density following the thermodynamic procedure developed in Refs. [48,54], we briefly outline the derivation of the NRHDE energy density, starting from the Rényi entropy associated

with a cosmological horizon of size L,

$$S_R = \frac{1}{\alpha}\ln(1+\alpha S_{\rm BH}), \qquad S_{\rm BH} = \frac{A}{4G} = \pi M_p^2 L^2. \tag{2}$$

Expanding the logarithm for small $\alpha S_{\rm BH}$ yields a controlled series in the Rényi deformation parameter,

$$S_R = S_{\rm BH} - \frac{\alpha}{2}S_{\rm BH}^2 + \frac{\alpha^2}{3}S_{\rm BH}^3 + \mathcal{O}(\alpha^3). \tag{3}$$

Following the standard thermodynamic/holographic construction adopted in Refs. [48,54] (see also analogous steps in Tsallis-type HDE models), the holographic dark energy density is obtained from the UV–IR relation $\rho_d \propto S_R/L^4$. Substituting the above expansion then leads to

$$\rho_d(L) = \frac{3c^2M_p^2}{L^2} - \frac{3}{2}c^2\alpha M_p^4 + c^2\alpha^2 M_p^6 L^2 + \mathcal{O}(\alpha^3), \tag{4}$$

which corresponds to Eq. (5) in the main text.

The truncation at $\mathcal{O}(\alpha^2)$ is physically well motivated. In fundamental (Planck) units, the Rényi deformation parameter α controls the departure from the Bekenstein–Hawking entropy and is expected to be small, so that retaining terms up to second order captures the leading Rényi-induced corrections beyond the standard HDE limit, while higher-order contributions $\mathcal{O}(\alpha^3)$ are subleading and are neglected in this work. For numerical integration and the figures presented below, we adopt code units $H_0 = 1$ and $M_p = 1$; in this normalization the parameter explored in the plots effectively corresponds to the rescaled combination $\hat{\alpha} \equiv \alpha M_p^2/H_0^2$. This truncation should therefore be understood as a controlled approximation within a phenomenological effective description, rather than as a fundamental series expansion of the underlying quantum-gravitational theory. Then yields the NRHDE energy density,

$$\rho_d = \frac{3c^2M_p^2}{L^2} - \frac{3}{2}c^2\alpha M_p^4 + c^2\alpha^2 M_p^6 L^2, \tag{5}$$

where M_p denotes the reduced Planck mass ($M_p^{-2} = 8\pi G$), while both c and α are dimensionless. Each term in ρ_d correctly carries the dimension of energy density, $[\rho_d] = \text{mass}^4$. The first term reproduces the conventional HDE density, the second acts as a constant shift, and the third introduces a positive correction scaling with L^2. Setting $\alpha = 0$ recovers the standard HDE result. We stress that the expansion in Eq. (5) originates from the entropy deformation encoded in the Rényi entropy and not from a derivative expansion in the Hubble parameter. Accordingly, no explicit $\dot{H}$ or higher-derivative terms appear at the level of the dark energy density; all time dependence enters indirectly through the evolution of the infrared cutoff L and the Friedmann equations.

The model is embedded in a spatially flat Friedmann–Robertson–Walker (FRW) background [8,17]. The Friedmann equations read

$$3M_p^2H^2 = \rho_m + \rho_d, \qquad -2M_p^2\dot{H} = \rho_m + \rho_d + p_d, \tag{6}$$

where ρ_m and ρ_d denote the matter and dark energy densities, respectively, and p_d is the pressure of NRHDE. According to the conservation equation, matter evolves as $\rho_m \propto a^{-3}$, and the dark energy component satisfies its own conservation equation. The fractional energy densities are defined as

$$\Omega_m = \frac{\rho_m}{3M_p^2H^2}, \quad \Omega_d = \frac{\rho_d}{3M_p^2H^2}, \quad \Omega_m + \Omega_d = 1. \tag{7}$$

From $\Omega_d = \rho_d/(3M_p^2H^2)$ and Eq. (5), one finds

$$\Omega_d = \frac{c^2}{H^2r_h^2} - \frac{1}{2}c^2\alpha\frac{M_p^2}{H^2} + \frac{c^2\alpha^2M_p^4}{3H^2}r_h^2, \tag{8}$$

where r_h is the future event horizon. For compactness, we now define

$$\mathcal{A} \equiv \frac{3}{2}c^2\alpha M_p^4 + 3M_p^2H^2\Omega_d, \qquad \mathcal{B} \equiv 12\,c^4\alpha^2M_p^8. \tag{9}$$

Multiplying through by $3M_p^2H^2r_h^2$ leads to a quadratic equation for r_h^2, following the same logic as in the standard HDE derivation [8],

$$c^2\alpha^2M_p^6r_h^4 - \mathcal{A}\,r_h^2 + 3c^2M_p^2 = 0. \tag{10}$$

whose physical solution is

$$r_h^2 = \frac{\mathcal{A} + \sqrt{\mathcal{A}^2 - \mathcal{B}}}{2c^2\alpha^2M_p^6}. \tag{11}$$

In the $\alpha \to 0$ limit, this reduces to the standard HDE relation

$$r_h = \frac{c}{H\sqrt{\Omega_d}}. \tag{12}$$

Reality of the root in Eq. (11) requires the discriminant to be non-negative. By taking $A = \frac{3}{2}c^2\alpha M_p^4 + 3M_p^2H^2\Omega_d$, the condition reads $A^2 \geq 12c^4\alpha^2M_p^8$. This inequality imposes a theoretical constraint on the Rényi parameter,

$$-\frac{3H^2\Omega_d}{M_p^2c^2(2\sqrt{3}+3/2)} \leq \alpha \leq \frac{3H^2\Omega_d}{M_p^2c^2(2\sqrt{3}-3/2)}. \tag{13}$$

It is essential to elucidate the physical meaning of this bound. In fundamental (Planck) units, the combination $H_0^2/M_p^2 \sim 10^{-122}$ is extremely small, so the microscopic parameter α appearing in Eq. (5) would indeed be tiny. However, in our numerical analysis the equations are solved in code units with ($H_0 = 1$, $M_p = 1$), which renders all quantities dimensionless and of order unity. Accordingly, we effectively probe the rescaled parameter

$$\hat{\alpha} \equiv \alpha\frac{M_p^2}{H_0^2}, \tag{14}$$

which controls the background evolution at the cosmological scale. In these units, the discriminant constraint becomes

$$-\frac{3\,E^2(z)\,\Omega_d}{c^2(2\sqrt{3}+3/2)} \le \hat{\alpha} \le \frac{3\,E^2(z)\,\Omega_d}{c^2(2\sqrt{3}-3/2)}, \tag{15}$$

where $E(z) = H(z)/H_0$. At $z = 0$ with $\Omega_{d0} \simeq 0.7$ and $c \simeq 0.9$, one obtains $\hat{\alpha} \in [-0.5, 1.3]$, which fully covers the range $\hat{\alpha} \sim \mathcal{O}(1)$ explored in our figures. Therefore, the apparent discrepancy between the microscopic and numerical scales arises from the adopted normalization, and the parameter values used in Sect. 3 are entirely consistent with the theoretical bounds.

The physically relevant solution corresponds to the positive root in Eq. (11), which smoothly recovers the standard HDE limit for $\alpha \to 0$. Moreover, requiring $\rho_d > 0$ throughout the cosmic evolution further favors non-negative α as the viable range employed in our numerical analysis. It is also instructive to note the asymptotic behavior of the energy density. At early times, when $L = r_h$ is small, the $1/L^2$ term dominates and the model effectively reduces to standard HDE. At late times, however, the $\propto L^2$ term becomes significant. For $\alpha > 0$ this enhances cosmic acceleration, whereas for large $|\alpha|$ the growth may be excessive. Thus late-time observations of $H(z)$ and $q(z)$ will be important to constrain α in future quantitative studies.

The time evolution of r_h is governed by

$$\dot{r}_h = Hr_h - 1, \qquad r_h = a\int_t^\infty \frac{dt'}{a(t')}. \tag{16}$$

It is worth emphasizing that Eq. (16) is a purely geometric relation that follows directly from the definition of the future event horizon and is therefore model-independent, as in the standard holographic construction [8,17]. By combining Eq. (16) with the explicit solution for r_h obtained from Eq. (11), we can express the horizon integral in a closed analytical form. This procedure is analogous to that used in the Tsallis holographic dark energy model [48,54], with the difference that the coefficients appearing here originate from the Rényi entropy density (Eq. (5)). The resulting expression reads

$$\int_x^\infty \frac{dx'}{Ha} = \frac{1}{a}\left[\frac{\mathcal{A}+\sqrt{\mathcal{A}^2-\mathcal{B}}}{2c^2\alpha^2M_p^6}\right]^{1/2}. \tag{17}$$

In the limit $\alpha \to 0$, Eq. (17) correctly reduces to the standard holographic result,

$$\int_x^\infty \frac{dx'}{Ha} = \frac{1}{a}\frac{c}{H\sqrt{\Omega_d}}, \tag{18}$$

which confirms the internal consistency of the NRHDE model. Using this integral relation together with Eq. (5), the differential equation for Ω_d can be obtained. After some algebra, one finds the closed form

$$\Omega_d' = \left[\left(-\frac{2c^2}{H^2r_h^3}+\frac{2c^2\alpha^2M_p^4}{3H^2}r_h\right)\left(r_h-\frac{1}{H}\right)+3\Omega_d\right] \times (1-\Omega_d), \tag{19}$$

where the prime denotes differentiation with respect to $x = \ln a = -\ln(1+z)$, with a the scale factor and z the redshift. This choice is particularly convenient because the evolution equations are often solved numerically in terms of x instead of cosmic time. In the $\alpha \to 0$ limit, Eq. (19) reduces to the well-known HDE equation [8],

$$\Omega_d' = \Omega_d(1-\Omega_d)\left(1+\frac{2}{c}\sqrt{\Omega_d}\right), \tag{20}$$

confirming the internal consistency of the NRHDE formulation. From the conservation equation, the equation-of-state (EoS) parameter of NRHDE is obtained as

$$w_d = -\frac{\Omega_d'}{3\,\Omega_d(1-\Omega_d)}. \tag{21}$$

In the standard HDE limit, this reduces to

$$w_d^{(\mathrm{HDE})} = -\frac{1}{3}-\frac{2}{3c}\sqrt{\Omega_d}. \tag{22}$$

Depending on the values of c and α, the NRHDE model can cross the phantom divide. The condition $w_d = -1$ is equivalent to $\Omega_d' = 3\Omega_d(1-\Omega_d)$, which, upon using Eq. (19), yields two distinct possibilities: either $r_h = 1/H$, corresponding to the exact de Sitter solution, or, for the specific NRHDE functional form given in Eq. (5), a Rényi-driven balance characterized by $r_h^4 = 3/(\alpha^2M_p^4)$. The latter relation demonstrates that the phantom crossing can dynamically emerge from the Rényi correction itself within this model. Ensuring the positivity of ρ_d at all epochs, particularly at late times when $\alpha < 0$, provides an additional physical consistency requirement. Finally, the deceleration parameter is given by

$$q = \frac{1}{2}\left(1+3w_d\Omega_d\right), \tag{23}$$

which explicitly illustrates the impact of Rényi corrections on late-time cosmic acceleration. The sign change of q indicates the transition from a decelerated to an accelerated expansion and highlights the potential of future observational data to place constraints on the non-extensivity parameter α within the NRHDE framework. For completeness, we note that our analysis is connected to the original HDE scenario in the smooth limit $\alpha \to 0$ [8], while more general entropy-inspired dark energy models can be found in Refs. [26,48,53,55].

3 Cosmological evolution of NRHDE

In Sect. 2 we derived the evolution equation for the NRHDE density parameter Ω_d, together with the corresponding expressions for the equation-of-state parameter w_d and the deceleration parameter q. In this section, we carry out a detailed numerical investigation of the background dynamics, examining how the Rényi deformation parameter α and the holographic constant c shape the cosmic expansion history. We specify the numerical setup and initial conditions, present the redshift evolution of $\Omega_d(z)$, $w_d(z)$, and $q(z)$, and discuss the resulting phenomenology in the light of the theoretical bounds derived in Sect. 2.

3.1 Numerical setup and initial conditions

The differential Eq. (19) is solved numerically by introducing the dimensionless e-folding variable

$$x = \ln a = -\ln(1+z), \tag{24}$$

where a is the scale factor and z is the redshift. Using x as the independent variable is particularly convenient, since it maps the entire cosmic history, from the early matter-dominated epoch ($x \to -\infty$, $z \gg 1$) to the asymptotic future ($x \to +\infty$, $z \to -1$), and improves the numerical stability of the evolution equations.

The present-day condition $\Omega_{d0} \simeq 0.7$ is imposed as the initial value at $x = 0$, which corresponds to $\Omega_{m0} \simeq 0.3$. We adopt code units with $H_0 = 1$ and reduced Planck units with $M_p^2 = 1$, and integrate the system over the redshift interval $-0.99 \le z \le 2.5$. Since the exact future limit $z = -1$ corresponds to $a \to \infty$ (or equivalently $x \to +\infty$), it cannot be reached in a finite numerical integration; the cutoff at $z = -0.99$ already captures the asymptotic late-time behaviour while ensuring numerical stability. For improved visualization of the early-time behaviour of the equation-of-state parameter, the $w_d(z)$ plots are extended to higher redshifts up to $z = 5$. Unless otherwise stated, the symbol α used in the figures denotes the rescaled parameter $\hat{\alpha} \equiv \alpha M_p^2/H_0^2$ introduced in Sect. 2.

3.2 Evolution of the density parameter

Figures 1 and 2 display the redshift evolution of the NRHDE density parameter $\Omega_d(z)$. In Fig. 1, the Rényi parameter is fixed at $\alpha = 0.4$, while the holographic parameter c varies in the range $0.5 \le c \le 1.5$. In Fig. 2, c is fixed at 0.9 and several values of α are examined.

In all cases, the NRHDE model reproduces the expected background evolution:

- $\Omega_d \to 0$ at high redshift ($z \gg 1$), corresponding to the matter-dominated era;

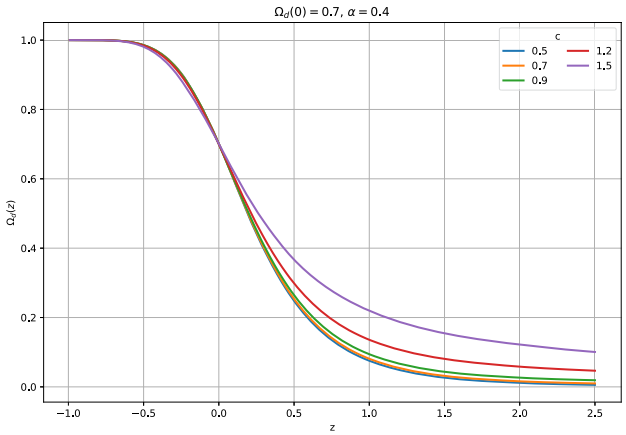

Fig. 1 Evolution of the NRHDE density parameter Ω_d versus redshift for fixed $\alpha = 0.4$ and holographic parameters $c = \{0.5, 0.7, 0.9, 1.2, 1.5\}$. All curves satisfy $\Omega_d(0) = 0.7$ with $M_p^2 = 1$. Increasing c delays the onset of dark-energy domination

- $\Omega_d(z=0) \simeq 0.7$, in agreement with the adopted present-day normalization;
- $\Omega_d \to 1$ as $z \to -1$, corresponding to the dark-energy-dominated epoch.

In practice, the exact asymptotic limit $z = -1$ corresponds to $a \to \infty$ and cannot be reached in a finite numerical integration. Throughout this work the future evolution is therefore followed numerically up to $z = -0.99$, which already captures the asymptotic late-time behaviour of the model with excellent accuracy.

Beyond this general trend, the parameters α and c distinctly shape the dynamics. At fixed α, decreasing c accelerates the rise of Ω_d and brings forward the onset of dark-energy domination, whereas increasing c delays this transition and yields a slower growth of Ω_d at late times. At fixed c, larger values of α enhance Ω_d at low redshift, reflecting the positive contribution of the $\propto \alpha^2 L^2$ term in Eq. (5). In the limit $\alpha \to 0$, the model continuously reduces to the standard HDE scenario.

3.3 Equation-of-state parameter evolution

Figures 3 and 4 display the redshift evolution of the NRHDE equation-of-state parameter $w_d(z)$. In Fig. 3, the Rényi parameter is fixed at $\alpha = 0.4$ while the holographic parameter c varies, whereas in Fig. 4, c is fixed at 0.9 and α is varied.

To make the asymptotic behaviour at both early and late times transparent, these figures are shown over the extended redshift interval $-0.99 \le z \le 5$. The exact future limit $z = -1$ corresponds to $a \to \infty$ and is therefore approached numerically by $z = -0.99$ (see the Numerical Setup in Sect. 3).

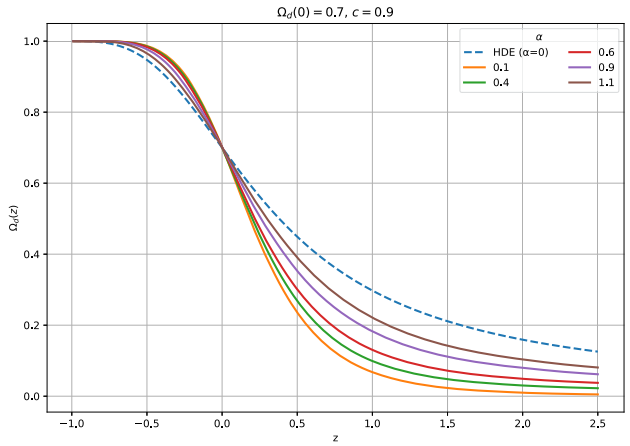

Fig. 2 Evolution of Ω_d versus redshift for fixed $c = 0.9$ and Rényi parameters $\alpha = \{0\,(\text{HDE}),\ 0.1,\ 0.4,\ 0.6,\ 0.9,\ 1.1\}$. Larger α enhances the late-time dark-energy contribution, leading to a faster approach toward $\Omega_d \simeq 1$ in the future

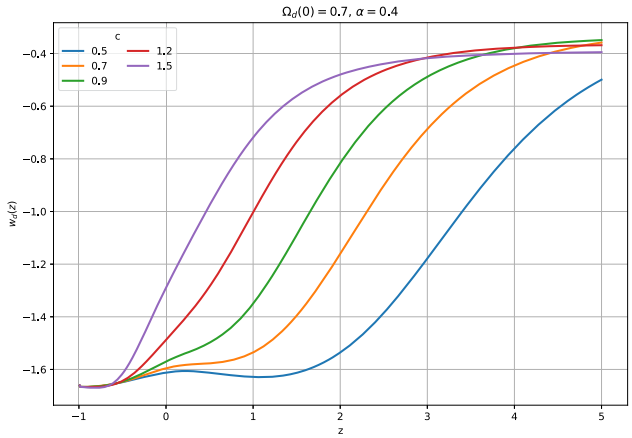

Fig. 3 Equation-of-state parameter $w_d(z)$ for fixed $\alpha = 0.4$ and $c = \{0.5, 0.7, 0.9, 1.2, 1.5\}$ with $\Omega_d(0) = 0.7$ and $M_p^2 = 1$, shown over the range $-0.99 \leq z \leq 5$

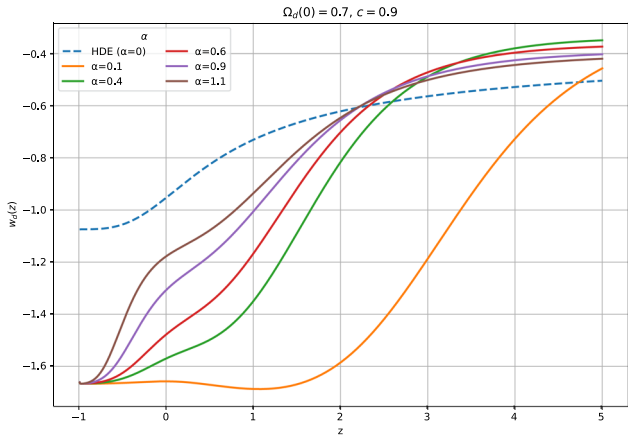

Fig. 4 Evolution of $w_d(z)$ for fixed $c = 0.9$ and $\alpha = \{0.1, 0.4, 0.6, 0.9, 1.1\}$ with $\Omega_d(0) = 0.7$ and $M_p^2 = 1$, shown over the range $-0.99 \leq z \leq 5$

For the representative parameter ranges shown in Figs. 3 and 4, the present-day equation-of-state parameter lies in the phantom regime, $w_{d0} < -1$, indicating that the NRHDE model can naturally realize a phantom phase at late times for a broad region of the parameter space. The strength of the phantom behaviour is controlled by the model parameters: larger values of c (at fixed α) or larger values of α (at fixed c) shift w_d upward, making the late-time evolution closer to the cosmological-constant boundary $w_d = -1$.

At sufficiently high redshift ($z \gtrsim \mathcal{O}(3)$–5 within the explored redshift range), all curves converge to $w_d \simeq -0.4$, reflecting the matter-dominated epoch where $\Omega_d \to 0$. In the asymptotic future ($z \to -1$), the curves tend to a constant value below -1 for the parameter sets displayed here, corresponding to a phantom-like late-time attractor. We emphasize that this transition is smooth and free of numerical instabilities within our integration scheme.

While Figs. 3 and 4 illustrate the late-time phantom behaviour along one-dimensional slices of the parameter space (varying either c or α at fixed values of the other), these behaviours are not contradictory. Rather, they correspond to different one-dimensional cuts through the same two-dimensional (c, α) parameter space. A complementary two-parameter analysis is therefore required to assess the global structure of the late-time dynamics.

To clarify the physical origin of the phantom-like behaviour observed in Figs. 3 and 4, Fig. 5 presents a two-dimensional representation of the present-day equation-of-state parameter, $w_{d0} \equiv w_d(z = 0)$, in the (c, α) parameter plane. This visualization provides a global view of the late-time dynamics by simultaneously varying the holographic parameter c and the Rényi deformation parameter α.

The colour map shows that the phantom regime, defined by $w_{d0} < -1$, occupies an extended and continuous region of the physically allowed parameter space, rather than being restricted to isolated parameter choices. In particular, the strongest phantom behaviour is realized for relatively small values of both parameters (approximately $c \lesssim 1$ and $\alpha \lesssim 0.4$), where w_{d0} reaches values as low as $w_{d0} \simeq -1.2$ to -1.3.

As either c or α is increased, the equation of state evolves smoothly toward the cosmological-constant boundary $w_{d0} \to -1$. Within the scanned domain shown in Fig. 5, this approach occurs from the phantom side, indicating that the late-time phantom phase emerges over a finite and well-defined region of the NRHDE parameter space.

3.4 Deceleration parameter and late-time dynamics

The behavior of the deceleration parameter $q(z)$ is shown in Figs. 6 and 7. The Universe evolves from a decelerated

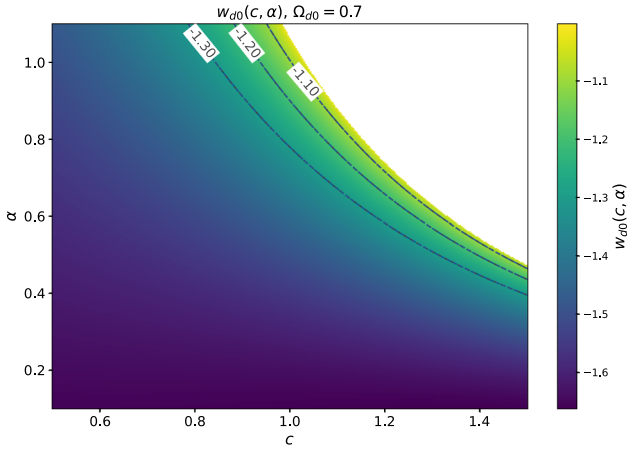

Fig. 5 Two-parameter map of the present-day equation-of-state parameter $w_{d0} \equiv w_d(z=0)$ in the (c,α) plane for $\Omega_{d0}=0.7$ and $H_0 = M_p = 1$. The colour scale shows the value of $w_{d0}(c,\alpha)$. The solid contour denotes the cosmological-constant boundary $w_{d0}=-1$. Within the scanned domain, the model remains in the phantom regime ($w_{d0}<-1$) and approaches $w_{d0}\to -1$ smoothly from below as either c or α increases

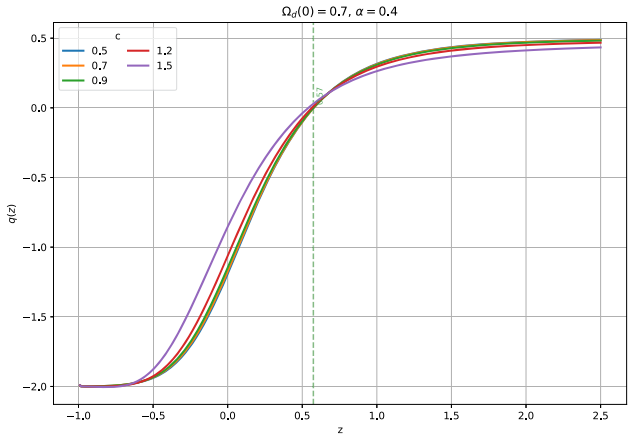

Fig. 6 Deceleration parameter $q(z)$ for fixed $\alpha = 0.4$ and $c = \{0.5, 0.7, 0.9, 1.2, 1.5\}$, shown over the range $-0.99 \le z \le 2.5$

expansion ($q>0$) during the matter-dominated era to an accelerated expansion ($q<0$) at late times.

For fixed $\alpha = 0.4$, the transition redshift from deceleration to acceleration, defined by $q(z_t)=0$, depends on the holographic parameter c. Smaller values of c shift the onset of acceleration to slightly higher redshift, while larger c tends to delay it. For representative values around $c \simeq 0.9$, the transition typically occurs at $z_t \simeq 0.55$–0.60, a range commonly discussed in the literature on late-time cosmic acceleration. At fixed $c=0.9$, increasing the Rényi deformation parameter α induces a mild shift of the transition toward higher redshift, indicating that stronger Rényi corrections can trigger cosmic acceleration slightly earlier.

In the asymptotic future, the deceleration parameter approaches $q\to -1$, corresponding to a de Sitter–like phase (numerically approached up to $z=-0.99$).

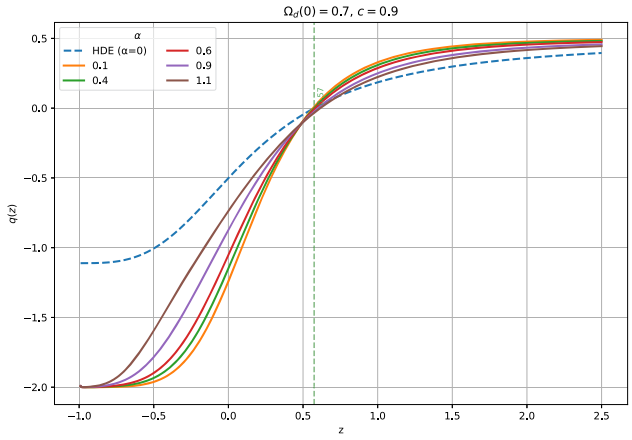

Fig. 7 Deceleration parameter $q(z)$ for fixed $c = 0.9$ and $\alpha = \{0\ (\text{HDE}), 0.1, 0.4, 0.6, 0.9, 1.1\}$. Vertical lines indicate the transition redshift z_t defined by $q(z_t)=0$. The curves are shown over $-0.99 \le z \le 2.5$

To visualise the joint impact of the two free parameters, Fig. 8 presents a two-dimensional map of the transition redshift $z_t(c,\alpha)$ in the (c,α) plane. The transition redshift is defined as the first zero-crossing of the deceleration parameter, $q(z_t)=0$, obtained from the background evolution.

For each parameter pair (c,α) in the scanned domain, the function $q(z)$ is computed over the interval $z\in[0,5]$, and the earliest redshift at which q changes sign from positive (deceleration) to negative (acceleration) is recorded as z_t. The colour scale represents the value of z_t, while the contour lines correspond to constant transition redshifts.

Within the explored parameter ranges, z_t varies smoothly over a relatively narrow interval, indicating a stable and continuous dependence on (c,α). Larger values of α generally shift the onset of acceleration to higher redshift, whereas larger c tends to delay it. The mild curvature of the contour lines reveals a genuine two-parameter interplay rather than a purely one-parameter dependence. Figures 6 and 7 can therefore be interpreted as one-dimensional slices of this two-dimensional surface.

3.5 Qualitative comparison with observational Hubble data

To provide a direct qualitative comparison between the NRHDE background evolution and late-time expansion measurements, we consider observational Hubble data (OHD) obtained with the cosmic chronometer (CC) method, where the Hubble parameter is inferred from the differential ageing of passively evolving galaxies. The CC compilation used in this work consists of 39 measurements in the redshift range $0.07 \lesssim z \lesssim 2.3$. For completeness, the full list of data points and their references are provided in Appendix A. All quoted uncertainties correspond to the 1σ confidence level.

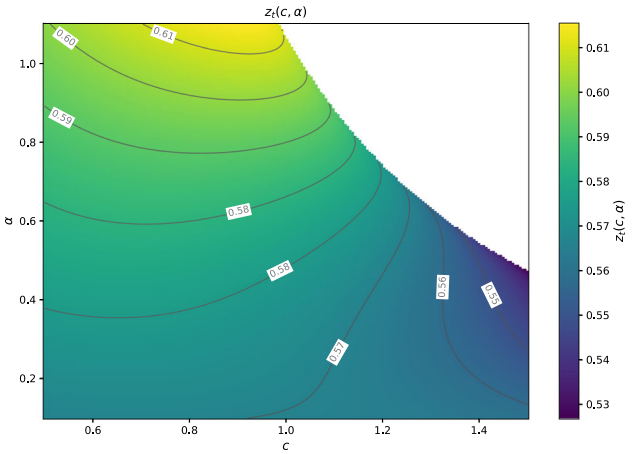

Fig. 8 Two-dimensional map of the transition redshift $z_t(c,\alpha)$ in the (c,α) plane for $\Omega_{d0} = 0.7$ and $H_0 = M_p = 1$. The transition redshift is defined by the first zero-crossing of the deceleration parameter, $q(z_t) = 0$. Colours and contour lines indicate constant values of z_t, which typically lie in the range $z_t \simeq 0.53$–0.61 over the scanned parameter space

In our numerical analysis, the background dynamics of the NRHDE model are fully characterized in terms of the dark-energy density parameter $\Omega_d(z)$. Combining the Friedmann equations, the explicit form of the NRHDE energy density, and the geometric relation for the future event horizon, the evolution equations can be recast into the closed first-order differential equation (19), which is solved numerically with the initial condition $\Omega_{d0} = 0.7$ at $z = 0$. Once $\Omega_d(z)$ is obtained, the Hubble expansion rate follows directly from the Friedmann constraint in a spatially flat universe.

Using $\Omega_m(z) = \Omega_{m0}(1+z)^3/E^2(z)$ together with $\Omega_m(z) + \Omega_d(z) = 1$, we obtain

$$E^2(z) \equiv \frac{H^2(z)}{H_0^2} = \frac{\Omega_{m0}(1+z)^3}{1-\Omega_d(z)}, \tag{25}$$

and therefore

$$H(z) = H_0\, E(z). \tag{26}$$

For visualization purposes only, a fiducial value of H_0 is adopted to convert the dimensionless prediction $E(z)$ into physical units km s^{-1} Mpc^{-1}. We emphasize that this choice serves solely to display the background evolution of $H(z)$ and does not involve any statistical fitting, parameter estimation, or inference of the present Hubble constant.

Figures 9 and 10 show the OHD points together with representative NRHDE predictions for selected values of the free parameters (c,α). At low redshifts ($z \lesssim 0.3$), all curves are nearly degenerate, indicating a weak sensitivity of the Hubble expansion rate to both parameters in the recent universe. The separation between different parameter choices becomes gradually more pronounced at $z \gtrsim 1$, demonstrating that both c and the Rényi parameter α mainly affect the background evolution at intermediate and high redshifts.

The lower panels display the fractional residuals $100 \times (H_{\rm mod} - H_{\rm OHD})/H_{\rm OHD}$, which remain typically within the $\pm(10-20)\%$ range over the full redshift interval and do not exhibit any strong systematic trend. This behavior suggests that the representative NRHDE background solutions are qualitatively consistent with the OHD compilation. A full likelihood analysis and a quantitative assessment of the model parameters are left for future work.

We stress that the apparent agreement at the background level should not be interpreted as a resolution of any existing cosmological tensions, but merely as a consistency check of the NRHDE framework with late-time expansion data.

4 Concluding remarks and outlook

In this work, we have developed the New Rényi Holographic Dark Energy (NRHDE) framework, which generalizes the standard holographic dark energy scenario by incorporating the logarithmic deformation of the Bekenstein–Hawking entropy encoded in the Rényi entropy formalism. Adopting the future event horizon as the infrared cutoff, we derived a modified holographic energy density and obtained a closed and self-consistent set of evolution equations for the density parameter Ω_d, the equation-of-state parameter w_d, and the deceleration parameter q. The model smoothly reduces to the conventional HDE in the limit $\alpha \to 0$, ensuring internal theoretical consistency.

Our numerical analysis shows that the NRHDE framework reproduces the essential qualitative features of late-time cosmology, including a matter-dominated past, a present epoch with $\Omega_{d0} \simeq 0.7$ (see Figs. 1–2), and a dark-energy-dominated future. Depending on the values of the parameters (c,α), the model realizes a phantom-like regime for the representative parameter choices shown in Figs. 3 and 4, with a smooth approach toward the cosmological-constant boundary $w_d = -1$ as either c or α increases.

The two-dimensional maps of the present-day equation-of-state parameter $w_{d0}(c,\alpha)$ and of the transition redshift $z_t(c,\alpha)$, shown in Figs. 5 and 8, provide a global characterization of the NRHDE parameter space. These representations demonstrate that both the phantom-like regime and the onset of cosmic acceleration arise over extended and continuous regions in (c,α), rather than being restricted to isolated parameter choices, and that the late-time dynamics result from the joint interplay between the holographic parameter c and the Rényi deformation parameter α.

We have also presented a qualitative comparison between the NRHDE background predictions and observational Hubble data obtained with the cosmic chronometer method (Figs. 9 and 10). This comparison illustrates that representative NRHDE solutions lead to expansion histories compatible with the observed $H(z)$ behaviour at the background level,

and should be interpreted solely as a consistency check rather than as a statistical test of the model.

A distinctive aspect of the present study is the direct derivation of the NRHDE evolution equations from the Rényi entropy formalism, providing a transparent link between horizon thermodynamics and cosmological dynamics. This establishes NRHDE as a minimal yet physically motivated extension of holographic dark energy, capable of capturing entropy-induced corrections at the background level without introducing additional dynamical degrees of freedom.

In future work, the NRHDE framework can be subjected to a comprehensive data-driven analysis. In particular, Bayesian parameter estimation based on combined CMB, BAO, Type Ia supernova, and observational Hubble data sets will allow quantitative constraints to be placed on the Rényi deformation parameter α. In parallel, implementing NRHDE perturbations within Boltzmann solvers such as CLASS or CAMB will enable a consistent treatment of structure formation and facilitate comparison with large-scale structure and weak-lensing observations.

From a theoretical perspective, exploring possible embeddings of NRHDE in modified-gravity or quantum-gravity–inspired scenarios may further clarify the connection between entropy, information, and the large-scale dynamics of spacetime. These extensions will provide a natural continuation of the present background-level analysis and help to assess the full observational viability of the NRHDE model in the era of precision cosmology.

Funding Open access funding was provided by SCOAP3.

Data Availability Statement Data will be made available on reasonable request. [Author's comment: The observational Hubble data used in this work are publicly available and have been properly cited in the article. No new datasets were generated during the current study.]

Code Availability Statement Code/software will be made available on reasonable request. [Author's comment: The code/software used to generate the figures and perform the analysis is available from the corresponding author upon reasonable request.]

Funded by SCOAP[3].

A Observational Hubble data

For completeness, we provide here the observational Hubble data compilation used for the qualitative comparison shown in Figs. 9 and 10. The dataset consists of 39 cosmic chronometer (CC, also referred to as the differential age or DA method) measurements spanning the redshift range $0.07 \lesssim z \lesssim 2.3$, with all uncertainties quoted at the 1σ confidence level.

For data sets in which separate statistical and systematic uncertainties or asymmetric error bars are reported in the original references (e.g. recent high-redshift CC measurements), the individual contributions have been combined in quadrature to construct an effective symmetric 1σ uncertainty. This treatment is adopted solely for visualization purposes in Figs. 9 and 10. The data presented here are not used

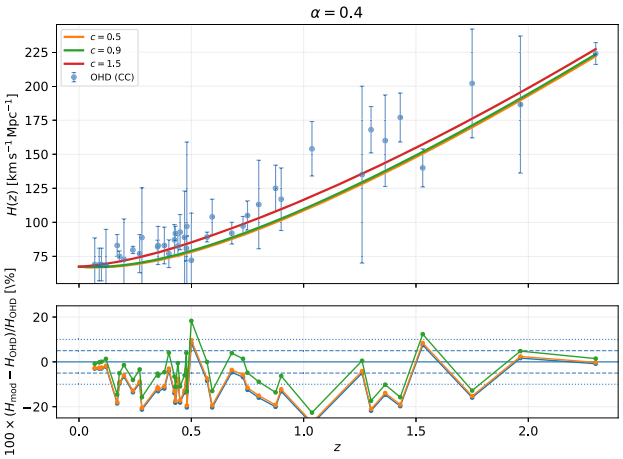

Fig. 9 Observational Hubble data (OHD) compared with NRHDE predictions $H(z)$ for fixed $\alpha = 0.4$ and different values of the holographic parameter $c = \{0.5, 0.9, 1.5\}$. The lower panel shows the fractional residuals $100 \times (H_{\rm mod} - H_{\rm OHD})/H_{\rm OHD}$

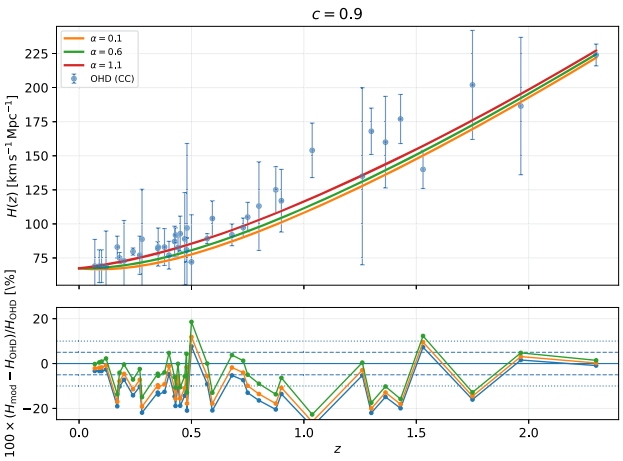

Fig. 10 Observational Hubble data (OHD) compared with NRHDE predictions $H(z)$ for fixed $c = 0.9$ and different values of the Rényi parameter $\alpha = \{0.1, 0.6, 1.1\}$. The lower panel shows the fractional residuals $100 \times (H_{\rm mod} - H_{\rm OHD})/H_{\rm OHD}$

Table 1 Cosmic chronometer (CC/DA) measurements of the Hubble parameter $H(z)$ (in km s^{-1} Mpc^{-1}) used for the qualitative comparison shown in Figs. 9 and 10. All uncertainties correspond to the 1σ confidence level. For data sets reporting separate statistical and systematic contributions or asymmetric errors, the uncertainties are combined in quadrature and shown as effective symmetric error bars. The data are not used for statistical fitting

z	$H(z)$	σ_H	Year	Ref	z	$H(z)$	σ_H	Year	Ref
0.070	69.00	19.60	2014	[56]	0.478	80.90	9.00	2016	[57]
0.090	69.00	12.00	2005	[58]	0.480	97.00	62.00	2010	[59]
0.100	69.00	12.00	2010	[59]	0.500	72.10	34.60	2025	[60]
0.120	68.60	26.20	2014	[56]	0.570	89.20	3.60	2012	[61]
0.170	83.00	8.00	2010	[59]	0.593	104.00	13.00	2012	[61]
0.180	75.00	4.00	2012	[61]	0.680	92.00	8.00	2012	[61]
0.200	72.90	29.60	2014	[56]	0.730	97.30	7.00	2012	[61]
0.240	79.69	2.65	2005	[58]	0.750	105.00	10.80	2023	[62]
0.270	77.00	14.00	2012	[61]	0.800	113.10	32.50	2022	[63]
0.280	88.80	36.60	2014	[56]	0.875	125.00	17.00	2012	[61]
0.350	82.10	4.80	2016	[57]	0.900	117.00	23.00	2010	[59]
0.352	83.00	14.00	2016	[57]	1.037	154.00	20.00	2012	[61]
0.380	83.00	13.50	2016	[57]	1.260	135.00	65.00	2023	[64]
0.400	77.00	10.20	2016	[57]	1.300	168.00	17.00	2012	[61]
0.425	87.10	11.20	2016	[57]	1.363	160.00	33.60	2015	[65]
0.429	91.80	5.30	2016	[57]	1.430	177.00	18.00	2015	[65]
0.440	82.60	7.80	2010	[59]	1.530	140.00	14.00	2010	[59]
0.450	92.80	12.90	2016	[57]	1.750	202.00	40.00	2010	[59]
0.470	89.00	34.00	2017	[66]	1.965	186.50	50.40	2015	[65]
					2.300	224.00	8.00	2015	[65]

for any statistical fitting, likelihood analysis, or parameter estimation (Table 1).

References

1. A.G. Riess et al., Title not provided. Astron. J. **116**, 1009–1038 (1998). https://doi.org/10.1086/300499. arXiv: astro-ph/9805201
2. S. Perlmutter et al., Title not provided. Astrophys. J. **517**, 565–586 (1999). https://doi.org/10.1086/307221. arXiv: astro-ph/9812133
3. K. Bamba, S. Capozziello, S. Nojiri, S.D. Odintsov, Title not provided. Astrophys. Space Sci. **342**, 155 (2012). https://doi.org/10.1007/s10509-012-1181-8. (**1205.3421**)
4. Collaboration, P., Aghanim, N., *et al.:* Planck 2018 results. vi. cosmological parameters. Astronomy & Astrophysics 641, 6 (2020) https://doi.org/10.1051/0004-6361/201833910arXiv:1807.06209 [arXiv: astro-ph.CO]
5. Collaboration, D., Adame, A.G., et al.: Desi 2024 results: Baryon acoustic oscillations from the first two years of desi observations. arXiv preprint (2024) arXiv:2404.03002 [arXiv: astro-ph.CO]
6. S. Nojiri, S.D. Odintsov, Title not provided. Gen. Relativ. Gravit. **38**, 1285–1304 (2006). https://doi.org/10.1007/s10714-006-0301-6
7. Copeland, E.J., Sami, M., Tsujikawa, S.: Dynamics of dark energy. International Journal of Modern Physics D 15(11), 1753–1936 (2006) https://doi.org/10.1142/S021827180600942X arXiv:hep-th/0603057 [hep-th]. Comprehensive review of dark energy models and their dynamics
8. M. Li, A model of holographic dark energy. Phys. Lett. B **603**, 1 (2004). https://doi.org/10.1016/j.physletb.2004.10.014
9. S.D.H. Hsu, Entropy bounds and dark energy. Phys. Lett. B **594**, 13 (2004). hep-th/0403052
10. L. Susskind, The world as a hologram. J. Math. Phys. **36**, 6377 (1995). https://doi.org/10.1063/1.531249. arXiv: hep-th/9409089
11. R. Bousso, The holographic principle. Rev. Mod. Phys. **74**, 825 (2002). hep-th/0203101
12. R. Horvat, Holographic bounds and dark energy. Physical Review D **70**, 087301 (2004). arXiv: astro-ph/0404204
13. Hooft, G.: Dimensional reduction in quantum gravity. In: Conf. Proc. C, vol. 930308, pp. 284–296 (1993)
14. J.D. Bekenstein, Black holes and entropy. Physical Review D **7**, 2333–2346 (1973). https://doi.org/10.1103/PhysRevD.7.2333
15. S.W. Hawking, Particle creation by black holes. Commun. Math. Phys. **43**, 199–220 (1975). https://doi.org/10.1007/BF02345020
16. S. Nojiri, S.D. Odintsov, Title not provided. European Physical Journal C **77**(8), 528 (2017). https://doi.org/10.1140/epjc/s10052-017-5097-x
17. S. Wang, Y. Wang, M. Li, Holographic dark energy: A review. Phys. Rep. **696**, 1–57 (2017). https://doi.org/10.1016/j.physrep.2017.06.003
18. C. Gao, X. Chen, Y.-G. Shen, Title not provided. Physical Review D **79**, 043511 (2009)
19. H. Hossienkhani, A. Aghamohammadi, A. Jafari, S.W. Rabieei, A. Refaei, Effects of low anisotropy on interacting holographic and new agegraphic scalar fields models of dark energy. Astrophys. Space Sci. **332**, 503–507 (2011). https://doi.org/10.1007/s10509-010-0531-7
20. A. Aghamohammadi, K. Saaidi, M.R. Setare, Holographic dark energy with time depend gravitational constant in the non-flat hořava-lifshitz cosmology. Physics of the Dark Universe **18**, 17–29 (2017). https://doi.org/10.1016/j.dark.2017.09.004
21. I. Duran, D. Pavon, Title not provided. Physical Review D **83**, 023504 (2011). https://doi.org/10.1103/PhysRevD.83.023504
22. R. Horvat, Holography and variable cosmological constant. Physical Review D **70**, 087301 (2004). https://doi.org/10.1103/PhysRevD.70.087301
23. B. Wang, C.-Y. Lin, E. Abdalla, Title not provided. Phys. Lett. B **637**, 357 (2006)
24. H.-C. Kao, W.-L. Lee, F.-L. Lin, Title not provided. Physical Review D **71**, 123518 (2005)
25. T.S. Biró, V.G. Czinner, Title not provided. Phys. Lett. B **726**, 861 (2013)

26. Rényi, A.: On measures of information and entropy. In: Proc. Fourth Berkeley Symposium on Mathematics, Statistics and Probability, pp. 547–561 (1961)
27. J.D. Barrow, Title not provided. Phys. Lett. B **808**, 135643 (2020). (**2004.09444**)
28. G. Kaniadakis, Title not provided. Phys. Rev. E **72**, 036108 (2005). (**cond-mat/0507311**)
29. M.T. Manoharan, N. Shaji, T.K. Mathew, Holographic dark energy from the laws of thermodynamics with rényi entropy. The European Physical Journal C **83**(1), 19 (2023). https://doi.org/10.1140/epjc/s10052-023-11202-w
30. D. Pavon, W. Zimdahl, Holographic dark energy and cosmic coincidence. Phys. Lett. B **628**, 206–210 (2005). https://doi.org/10.1016/j.physletb.2005.08.134gr-qc/0505020
31. M.-J. Zhang, C. Ma, Z.-S. Zhang, Z.-X. Zhai, T.-J. Zhang, Title not provided. Physical Review D **88**, 063534 (2013)
32. J.-F. Zhang, M.-M. Zhao, Y.-H. Li, X. Zhang, Title not provided. J. Cosmol. Astropart. Phys. **1504**, 038 (2015)
33. M.T. Manoharan, Entropy bounds and holographic dark energy: Conflicts and consensus. Ann. Phys. **482**, 170231 (2025). https://doi.org/10.1016/j.aop.2025.170231
34. A. Mehrabi, S. Basilakos, M. Malekjani, Z. Davari, Title not provided. Physical Review D **92**, 123513 (2015)
35. Q.-G. Huang, Y.-G. Gong, Title not provided. J. Cosmol. Astropart. Phys. **0408**, 006 (2004)
36. C. Tsallis, Possible generalization of boltzmann-gibbs statistics. J. Stat. Phys. **52**, 479 (1988)
37. N. Drepanou, A. Lymperis, E.N. Saridakis, K. Yesmakhanova, Title not provided. European Physical Journal C **82**, 449 (2022). https://doi.org/10.1103/PhysRevD.83.023504. (**2109.09181**)
38. B.D. Pandey et al., Title not provided. European Physical Journal C **82**, 233 (2022). https://doi.org/10.1140/epjc/s10052-022-10171-w
39. Rényi, A.: Proceedings of the 4th berkeley symposium on mathematics, statistics and probability. In: Proc. 4th Berkeley Symp. Math. Stat. Prob., vol. I, p. 547. University of California Press, Berkeley and Los Angeles (1960)
40. A. Mohammadi et al., Title not provided. Physical Review D **103**, 083505 (2021)
41. B.C. Paul, P. Thakur, A. Saha, Cosmology with sharma-mittal holographic dark energy. Phys. Lett. B **720**, 389–393 (2013). https://doi.org/10.1016/j.physletb.2013.02.040
42. Nojiri, S., Odintsov, S.D., Faraoni, V.: Title not provided. Physical Review D 104, 084030 (2021) https://doi.org/10.1103/PhysRevD.104.084030 2109.05315. See also: Phys. Rev. D 105, 044042 (2022), 2201.02424; Int. J. Geom. Meth. Mod. Phys. 19, 2250210 (2022), 2207.07905
43. S.D. Odintsov, T. Paul, Title not provided. Physics of the Dark Universe **39**, 101159 (2023). (**2212.05531**)
44. A. Khodam-Mohammadi, M. Monshizadeh, Cosmological tensions with non-extensive entropic cosmology: a modified stress-energy approach. The European Physical Journal C **85**(9), 1072 (2025). https://doi.org/10.1140/epjc/s10052-025-14824-4
45. Li, M., Wang, Y., Wang, S., Zhang, J.: Revisiting holographic dark energy after desi 2024: constraints from updated bao and hubble data. European Physical Journal C 85, 279 (2025) https://doi.org/10.1140/epjc/s10052-025-14279-7 . Based on DESI 2024 BAO results
46. Dąbrowski, M.P., Atreya, F., Balcerzak, A.: Generalized non-extensive entropy holographic dark energy models verified by cosmological data. European Physical Journal C 85, 498 (2025) https://doi.org/10.1140/epjc/s10052-025-14498-y . Non-extensive entropy models with observational constraints
47. A. Khodam-Mohammadi, M. Monshizadeh, Title not provided. Phys. Lett. B **843**, 138066 (2023)
48. A. Sheykhi, Modified friedmann equations from tsallis entropy. Phys. Lett. B **785**, 118 (2018)
49. A. Pandey, P. Kumar, S. Kumar, New tsallis holographic dark energy model with future event horizon cutoff. European Physical Journal C **82**, 355 (2022). https://doi.org/10.1140/epjc/s10052-022-10326-4
50. B. Pourhassan, A. Bonilla, M. Faizal, E.M.C. Abreu, Title not provided. Physics of the Dark Universe **20**, 41–48 (2018). https://doi.org/10.1016/j.dark.2018.02.006
51. V.G. Czinner, H. Iguchi, Title not provided. Universe **3**(1), 14 (2017)
52. H. Moradpour, S.A. Moosavi, I.P. Lobo, J.P.M. Graça, A. Jawad, I.G. Salako, Thermodynamic approach to holographic dark energy and the rényi entropy. The European Physical Journal C **78**(10), 829 (2018). https://doi.org/10.1140/epjc/s10052-018-6309-8
53. S. Nojiri, S.D. Odintsov, E.N. Saridakis, Modified cosmology from extended entropy with varying exponent. European Physical Journal C **79**, 242 (2019)
54. A.S. Jahromi, S.A. Moosavi, H. Moradpour, J.P.M. Graça, I.P. Lobo, I.G. Salako, A. Jawad, Title not provided. Phys. Lett. B **780**, 21 (2018). (**1802.07722**)
55. S. Wang, Y. Wang, M. Li, Holographic dark energy: A review. Phys. Rep. **696**, 1 (2023)
56. C. Zhang, H. Zhang, S. Yuan et al., Four new observational h(z) data from luminous red galaxies in the sloan digital sky survey data release seven. Res. Astron. Astrophys. **14**(10), 1221–1233 (2014). https://doi.org/10.1088/1674-4527/14/10/002
57. Moresco, M., *et al.:* A 6% measurement of the hubble parameter at $z \sim 0.45$: direct evidence of the epoch of cosmic re-acceleration. J. Cosmol. Astropart. Phys. 2016(05), 014 (2016) https://doi.org/10.1088/1475-7516/2016/05/014
58. J. Simon, L. Verde, R. Jimenez, Constraints on the redshift dependence of the dark energy potential. Phys. Rev. D **71**, 123001 (2005). https://doi.org/10.1103/PhysRevD.71.123001
59. Stern, D., Jimenez, R., Verde, L., Kamionkowski, M., Stanford, S.A.: Cosmic chronometers: constraining the equation of state of dark energy. i: H(z) measurements. J. Cosmol. Astropart. Phys. 2010(02), 008 (2010) https://doi.org/10.1088/1475-7516/2010/02/008
60. S.I. Loubser et al., Cosmic chronometers with bcgs: new measurements of h(z) using d4000n indices. Mon. Not. R. Astron. Soc. **523**(4), 6171–6186 (2025). https://doi.org/10.1093/mnras/staf915
61. Moresco, M., *et al.:* Improved constraints on the expansion rate of the universe up to $z \sim 1.1$ from the spectroscopic evolution of cosmic chronometers. J. Cosmol. Astropart. Phys. 2012(08), 006 (2012) https://doi.org/10.1088/1475-7516/2012/08/006
62. R. Jimenez, M. Moresco, L. Verde, B.D. Wandelt, Photometric cosmic chronometers: a new route to h(z). J. Cosmol. Astropart. Phys. **2023**(07), 013 (2023). https://doi.org/10.1088/1475-7516/2023/07/013
63. K. Jiao, N. Borghi, M. Moresco et al., Cosmic chronometers with full spectral fitting of passive galaxies in lega-c. Astron. Astrophys. **665**, 101 (2022). https://doi.org/10.1051/0004-6361/202243494
64. E. Tomasetti, M. Moresco et al., Extending cosmic chronometers to high redshift with vandels: New constraints on h(z). Astron. Astrophys. **675**, 74 (2023). https://doi.org/10.1051/0004-6361/202346112
65. M. Moresco, Raising the bar: new constraints on the hubble parameter with cosmic chronometers at $z \sim 2$. Mon. Not. R. Astron. Soc. **450**(1), 16–20 (2015). https://doi.org/10.1093/mnrasl/slv037
66. A.L. Ratsimbazafy et al., Age-dating luminous red galaxies observed with the southern african large telescope. Mon. Not. R. Astron. Soc. **467**(3), 3239–3254 (2017). https://doi.org/10.1093/mnras/stx301